

A Saliency-based Convolutional Neural Network for Table and Chart Detection in Digitized Documents

I. Kavasidis, S. Palazzo, C. Spampinato, C. Pino, D. Giordano, D. Giuffrida, P. Messina

Abstract—Deep Convolutional Neural Networks (DCNNs) have recently been applied successfully to a variety of vision and multimedia tasks, thus driving development of novel solutions in several application domains. Document analysis is a particularly promising area for DCNNs: indeed, the number of available digital documents has reached unprecedented levels, and humans are no longer able to discover and retrieve all the information contained in these documents without the help of automation. Under this scenario, DCNNs offers a viable solution to automate the information extraction process from digital documents. Within the realm of information extraction from documents, detection of tables and charts is particularly needed as they contain a visual summary of the most valuable information contained in a document. For a complete automation of visual information extraction process from tables and charts, it is necessary to develop techniques that localize them and identify precisely their boundaries.

In this paper we aim at solving the table/chart detection task through an approach that combines deep convolutional neural networks, graphical models and saliency concepts. In particular, we propose a saliency-based fully-convolutional neural network performing multi-scale reasoning on visual cues followed by a fully-connected conditional random field (CRF) for localizing tables and charts in digital/digitized documents.

Performance analysis carried out on an extended version of ICDAR 2013 (with annotated charts as well as tables) shows that our approach yields promising results, outperforming existing models.

Index Terms—Document Analysis, Semantic Image Segmentation, Object Detection

I. INTRODUCTION

Production and storage of digital documents have increased exponentially in the last two decades. Extracting and retrieving information from this massive amount of data have become inaccessible to human operators and a large amount of information captured in digital documents may go lost or never seen. As a consequence, a large body of research has focused on automated methods for document analysis. Most of these efforts are directed towards the development of Natural Language Processing (NLP) methods, that analyze both grammar and semantics of text with the goal of automatically extracting, understanding and, eventually, summarizing key information from digital documents. However, while text is, inarguably, a fundamental way to convey information, there are contexts where graphical elements are much more powerful.

For example, in scientific papers, many experiments, variables and numbers need to be reported in a concise way that fits better with tables/figures than text. The idiom “*a picture is worth a thousand words*” describes exhaustively the power that graphical elements possess in conveying information that would be otherwise cumbersome, both for the writer to express and the reader to understand. Thus, it is of primary importance for an effective automatic document processing approach to gather information from tables and charts. Several commercial software products that convert digitized and digital documents into processable text already exist. However, most of them either largely fail when dealing with graphical elements or require an exact localization of such elements to work properly. For this reason, a crucial pre-processing step in automated data extraction from tables and charts is to find their exact location.

The problem of identifying objects in images traditionally falls in the object detection research area, where, nowadays, Deep Convolutional Neural Networks (DCNNs) play the leading role [1], [2]. However, naively employing DCNN-based object detectors in digital documents, suitably transformed into images, leads to failures mainly because of the intrinsic appearance difference between digital documents and natural images (the data for which models are mainly thought for). Trying to train models from scratch may be unfeasible due to the large number of images required and to the lack of suitably annotated document datasets. Moreover, such approaches generally exploit the visual differences between object categories: while the visual characteristics of certain graphical elements (e.g., charts) significantly differ from text, the same cannot be said for tables, whose main differences from the surrounding content lie mostly in the layout. Finally, many of the existing object detectors are often prone to potential errors by upstream region proposal models and are not able to detect simultaneously all the objects of interest in an image [3], [4].

For all these reasons, traditional object detectors may be inappropriate to perform accurate table and chart detection/segmentation. Given our previous consideration on how tables are identifiable mostly by their layout than by their content (which is still textual), a possible solution would be that of posing the problem as a *saliency detection* one. Saliency is the perceptual quality of certain objects (or object parts) that possess distinctive features with respect to the surroundings: such salient characteristics may not be very different from other elements in the scene, but may attract the viewer’s attention through aspects such as, for example, arrangement [5]. This definition seems particularly appropriate to tables, whose organized structure easily stands out in a page otherwise filled with an unstructured flow of text. We argue

I. Kavasidis, S. Palazzo, C. Spampinato, C. Pino and D. Giordano are with the Pattern Recognition and Computer Vision (PeRCeiVe) Lab at the University of Catania, in Italy, email: (see www.perceivelab.com). D. Giuffrida and P. Messina are with Tab2Ex company, San Jose’, California (USA), see <http://www.tab2ex.com/> and <https://snapchart.co>.

Manuscript submitted April 13, 2018

that identifying local (i.e., pixelwise) patterns such as lines and spacings that characterize the presence of a table is the key to localizing the whole object. In our case, however, we focus on different objects (not only tables, but also charts) and thus we have different types of saliency, corresponding to the targeted object categories: from this point of view, the problem becomes one of *semantic segmentation*, i.e., assigning a class to each pixel in an image.

DCNN-based object detection methods have been repurposed for semantic segmentation by leveraging the learned low and middle level region representations. However, the multi-scale aggregation and down-sampling employed by DCNNs for object detection show several drawbacks when performing dense prediction, which, instead, requires multi-scale reasoning at high image resolution [6]. In other words, the responses at the final layers of CNN-based object detection methods are not localized enough for pixelwise classification because their invariance properties make them more suitable for high level tasks. This limitation is particularly problematic for table detection, where long-range dependencies are essential to distinguish between, for example, two horizontally-stacked tables or two groups of columns of the same table (and analogously in the vertical direction).

In this paper we propose a fully-convolutional neural network for table and chart detection able to overcome the limitations of the existing approaches. In detail, we frame our approach as a semantic image segmentation one, i.e., we perform pixelwise dense prediction assigning to each pixel a likelihood of being part of an object of interest. In order to capture long-term dependencies between elements in a document, our network exploits dilated convolutions [6] for effectively extracting and using multi-scale contextual information in a dense prediction problem. Since tables and charts are among the most salient (according to visual saliency definition) areas in an image, our network is first pre-trained on saliency detection datasets to learn basic visual cues and afterwards fine-tuned on digital documents. Additionally, in order to provide a stronger supervision to the internal saliency detectors, we employ the approach introduced in [7], by adding a loss term related to the capability of the saliency maps to identify regions that are distinctive for visual classification in one of the four target categories. Finally, predictions of our network are enhanced with a fully connected Conditional Random Field (CRF) [8].

Performance evaluation, carried out on an extended version of ICDAR 2013 dataset (with annotated charts as well as tables), reveals that our network significantly outperforms other DCNN models as well as state-of-the-art methods in detecting tables and charts in digital documents.

The paper is organized as follows: in the next section a review of the literature on table detection/classification is presented, while in Section III our saliency-based semantic segmentation approach is described. In Section IV, we report the results yielded by our approach on the extended ICDAR 2013 dataset, and in the final section conclusions are drawn and future directions given.

II. RELATED WORK

Given the large quantity of digital documents that are available today, it is mandatory to develop automatic approaches to extract, index and process information for long-term storage and availability. Consequently, there is a large body of research on document analysis methods attempting to extract different types of objects (e.g., tables, charts, pie charts, etc.) from various document types (text documents, source files, documents converted into images, etc.).

Before the advent of deep learning, most works on document analysis for table detection were based on exploiting *a priori* knowledge on object properties by analyzing tokens extracted from source document files [9], [10], [11], [12], [13]. For example, [10] proposes a method for table detection in PDF documents, which uses tags of tabular separators to identify the table region. Similarly, in [11], tables are detected by thoroughly analyzing the page layout and searching for tab-stop tokens (i.e., vertical lines that delimit areas of text), which are then combined to see if they match a set of predefined criteria related to tabular shape and, accordingly, to decide whether a candidate area is a table or not. Of course, the main shortcoming of all methods that rely on detecting horizontal or vertical lines for table detection is that they fail to identify tables without borders. Alternatively, methods operating on image conversion of document files and exploiting only visual-cues for table detection have been proposed [14], [15], [16], [17], [18]. For example, [15] describes an approach for extracting tables from web documents without searching for HTML *table* tags, instead using visual cues and heuristic rules. However, methods of this kind have shown rather limited performance for specific table categories [16], [17], [18] and are not general enough for consumer market. Similar computer vision-based methods have been proposed for detecting other types of graphical elements (e.g., charts, diagrams, etc.) than tables [19], [20], [21]. These methods basically employ simple computer vision techniques (e.g., connected components, fixed set of geometric constraints, edge detection, etc.) to extract chart images, but, as for the table detection case, they show scarce generalization capabilities. Low-level visual cues (e.g., intensity, contrast, homogeneity, etc.) in combination with shallow machine learning techniques have been used for specific object classification tasks [22], [23] with fair performance, but these methods are mainly for classification as they tend to aggregate global features in compact representations which are less suitable for performing object detection. Performance improvement has been also sought by resorting to graphical models [24], [25], [26]) such as Conditional Random Fields (CRFs), but despite their capabilities to capture fine edge details, these methods are still not as effective as expected. Our hypothesis is that the main reason for unsatisfactory performance is that tables (mainly) and charts usually cover large areas and, as such, they need methods able to account for long-range dependencies.

in [26], Conditional Random Fields are used to label table rows in government style documents and extract the data represented achieving almost perfect performance (> 95%), but the main drawbacks are the simplicity of the layout and

the strict adherence to a specific document template.

With the recent rediscovery of deep learning, in particular convolutional neural networks, and its superior representation capabilities for high-level vision tasks, the document analysis research community started to employ DCNNs for document processing, with a particular focus on document classification [27], [28], [29], [30] or object (mainly chart) classification – after accurate manual detection [31], [32]. One recent work presenting a DCNN exclusively targeted to table detection is [33], which employs Faster R-CNN [3] for object detection. Nevertheless, this method suffers from the limitations mentioned in the previous section, i.e., its performance is negatively affected by the region proposal mistakes and it does not provide multiple detections for each image [34]. In this paper, we tackle the table and chart detection problem from a different perspective, i.e., we pose it as semantic image segmentation problem, by densely predicting — according to visual saliency principles — for each pixel of the input image the likelihood of being part of a set of predefined classes. Despite contributing to the semantic image segmentation and saliency detection fields is out of the scope of this paper, we review briefly the state of the art on the two topics to provide the reader a means to understand the CNN architectural choices discussed in the next section.

Saliency detection is a long researched topic and it aims at reproducing the human early unconscious process for scanning a visual scene through an attention mechanism guided by some coarse visual stimuli, followed by a late top-down process biasing the observation towards those regions that consciously attract human attention according to a specific task. The literature on this topic is large [35], [36], [37], [38], [39], [40], [41], [39], and the current state of the art [42], [37] is oriented to fully-convolutional CNN architectures processing images at different scales for dense saliency prediction of each pixel. In addition, driving fully-convolutional CNN saliency detectors with specific goals results in improved detection performance [43], [7].

Semantic image segmentation is, instead, the task of assigning a label from a set of classes to each pixel of the image. It has been widely investigated in past years with methods aiming at finding a graph structure over the image to capture the context of each pixel by using Markov Random Fields (MRF) or Conditional Random Fields (CRF) [44]. However, these methods employ hand-crafted features for classification, thus do not generalize well. Recently, the problem has been tackled by proposing fully-convolutional networks obtained by transforming fully-connected layers of pre-trained CNNs into convolutional layers. These methods, though more effective than traditional approaches, suffer from the scarce representation capabilities of pre-trained CNN-based classifiers for dense prediction. Indeed, they tend to create compact embeddings, via pooling and subsampling layers that aggregate multi-scale contextual information for global prediction, while dense prediction requires an explicit link between context information and pixel-wise prediction.

In this paper, we borrow methods from both research topics and propose a DCNN-based fully-convolutional approach, which exploits their respective potentialities improving, at the

same time, their limitations. In detail, our approach employs a fully-convolutional architecture designed to perform semantic segmentation in a way that, through dilated convolutions [6], makes an explicit assumption on the link between context information and dense prediction. This architecture is adapted to compute heatmaps containing pixelwise scores of how salient each pixels is with respect to K possible object classes. In order to drive the model to highlight not only salient regions (which may be distinctive but sparse) but also the whole area of a target object, we jointly train a set of binary classifiers that employ the computed saliency maps to correctly classify regions of the input images, thus causing the classification loss to be propagated to the saliency detectors as an additional error signal [7]. Finally, we enhance the output maps of object location with the fully connected CRF proposed in [8].

III. DEEP LEARNING MODELS FOR TABLE AND CHART DETECTION AND CLASSIFICATION

The approach for table and chart extraction presented here works by receiving an image as input and generating a set of binary masks as output, from which bounding boxes are drawn. Each binary mask corresponds to the pixels that belong to objects of four specific classes: *tables*, *pie charts*, *line charts* and *bar charts*. An example of the expected outputs is shown in Fig. 1. The main processing engine driving our approach consists of a fully-convolutional deep learning model that performs table/chart detection and classification, followed by a conditional random field for enhancing and smoothing the binary masks (see Fig. 2).

A. Table and chart extraction and classification

Given an input document page transformed into an RGB image and resized to 300×300 , the output of the system consists of four binary masks, one for each of the aforementioned classes. Pixels set to 1 in a binary mask identify document regions belonging to instances of the corresponding class, while 0 values are background regions (e.g., regular text).

We leverage visual saliency prediction to solve our object detection problem. As a result, the first processing block in our method is a fully-convolutional neural network (i.e., composed only by convolutional layers [45]) that extracts four class-specific heatmaps from document images.

Our saliency detection network is based on the feature extraction layers of the VGG-16 [46] architecture. However, we applied a modification aimed at exploiting inherent properties of tables and charts: in particular, the first two convolutional layers do not employ traditional square convolution kernels, as in the original VGG-16 implementation, but use rectangular ones instead, of sizes 3×7 and 7×3 (equally distributed in the number of feature maps for each layer, see Table I). This set up gives our network the ability to extract table-related features (e.g., lines, spacings, columns and rows) even at the early stages. Padding was suitably added in order to keep the size of the output feature maps independent of the size of the kernels.

After the cascade of layers from the VGG-16 architecture, the resulting 75×75 feature maps are processed by a *dilation block*, consisting of a sequence of dilated convolutional

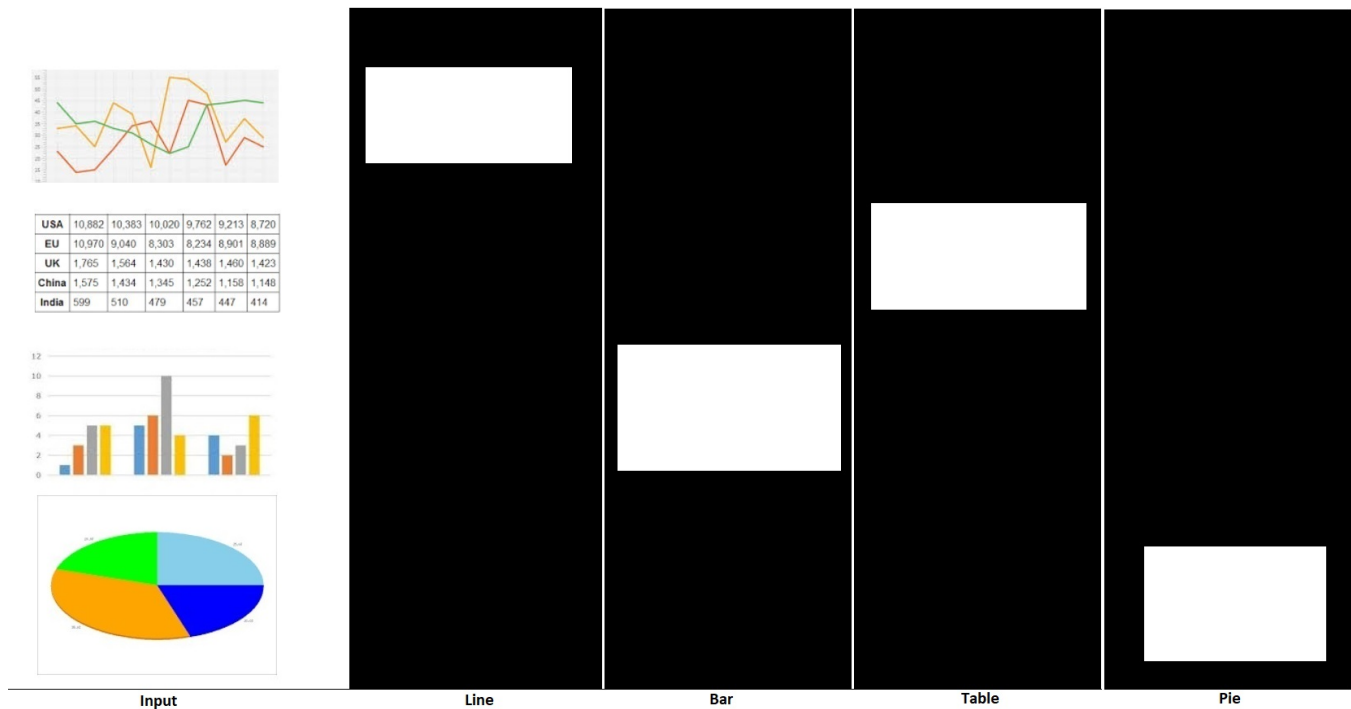


Fig. 1. An example input image (first image, left) and the corresponding desired outputs (binary images, right).

TABLE I
ARCHITECTURAL DETAILS OF THE SALIENCY DETECTION NETWORK. ALL CONVOLUTIONAL LAYERS EXCEPT THE LAST ONE ARE FOLLOWED BY BATCH NORMALIZATION LAYERS AND RELU ACTIVATIONS.

Layer	Maps	Kernel size	Stride	Pad	Dilation
Conv	64	$3 \times 7, 7 \times 3$	1×1	$1 \times 3, 3 \times 1$	1×1
Conv	64	$3 \times 7, 7 \times 3$	1×1	$1 \times 3, 3 \times 1$	1×1
MaxPool	-	2×2	2×2	-	-
Conv	128	3×3	1×1	1×1	1×1
Conv	128	3×3	1×1	1×1	1×1
MaxPool	-	2×2	2×2	-	-
Conv	256	3×3	1×1	1×1	1×1
Conv	256	3×3	1×1	1×1	1×1
Conv	256	3×3	1×1	1×1	1×1
Conv	512	3×3	1×1	1×1	1×1
Conv	512	3×3	1×1	1×1	1×1
Conv	512	3×3	1×1	1×1	1×1
Conv	512	3×3	1×1	1×1	1×1
Conv	512	3×3	1×1	1×1	1×1
Conv	512	3×3	1×1	1×1	1×1
DilConv	512	3×3	1×1	1×1	2×2
DilConv	512	3×3	1×1	1×1	4×4
DilConv	512	3×3	1×1	1×1	8×8
DilConv	512	3×3	1×1	1×1	16×16
Conv	256	3×3	1×1	1×1	1×1
Conv	4	1×1	1×1	-	1×1

layers [6]. While the purpose of the previous layers is that of extracting discriminative local features, the dilation block exploits dilated convolutions to establish multi-scale and long-range relations. Dilation layers increase the receptive field of convolutional kernels while keeping the feature maps at a constant size, which is desirable for pixelwise dense prediction as we do not want to spatially compact features further. The output of the dilation block is a 4-channel feature map,

where each channel is the saliency heatmap for one of the target object categories. After the final convolutional layer, we upsample the 75×75 maps back to the original 300×300 using bilinear interpolation.

In theory, the saliency maps could be the only expected output of the model, and we could train it by just providing the correct output as supervision. However, [7] recently showed that posing additional constraints to saliency detection — for example, forcing the saliency maps to identify regions that are also class-discriminative — improves output accuracy. This is highly desirable in our case as output saliency maps may miss non-salient regions (e.g., regular text) inside salient regions (e.g., table borders), while it is preferable to obtain maps that entirely cover the objects of interest.

For this reason, we add a classification branch to the model. This branch contains as many binary classifiers as the number of target object classes. Each binary classifier receives as input a crop of the original image around an object (connected component) in the saliency detector outputs, and aims at discriminating whether that crop contains an instance of target class. The classifiers are based on the Inception model [47] and are architecturally identical, except for the final classification layer which is replaced by a linear layer with one neuron followed by a sigmoid nonlinearity.

B. Multi-loss training

To train the model we employ a multi-loss function that combines the error measured on the computed saliency maps with the classification error of the binary classifiers. The saliency loss function measured between the computed saliency maps \mathbf{Y} (expressed as a $N \times 300 \times 300$ tensor, with N

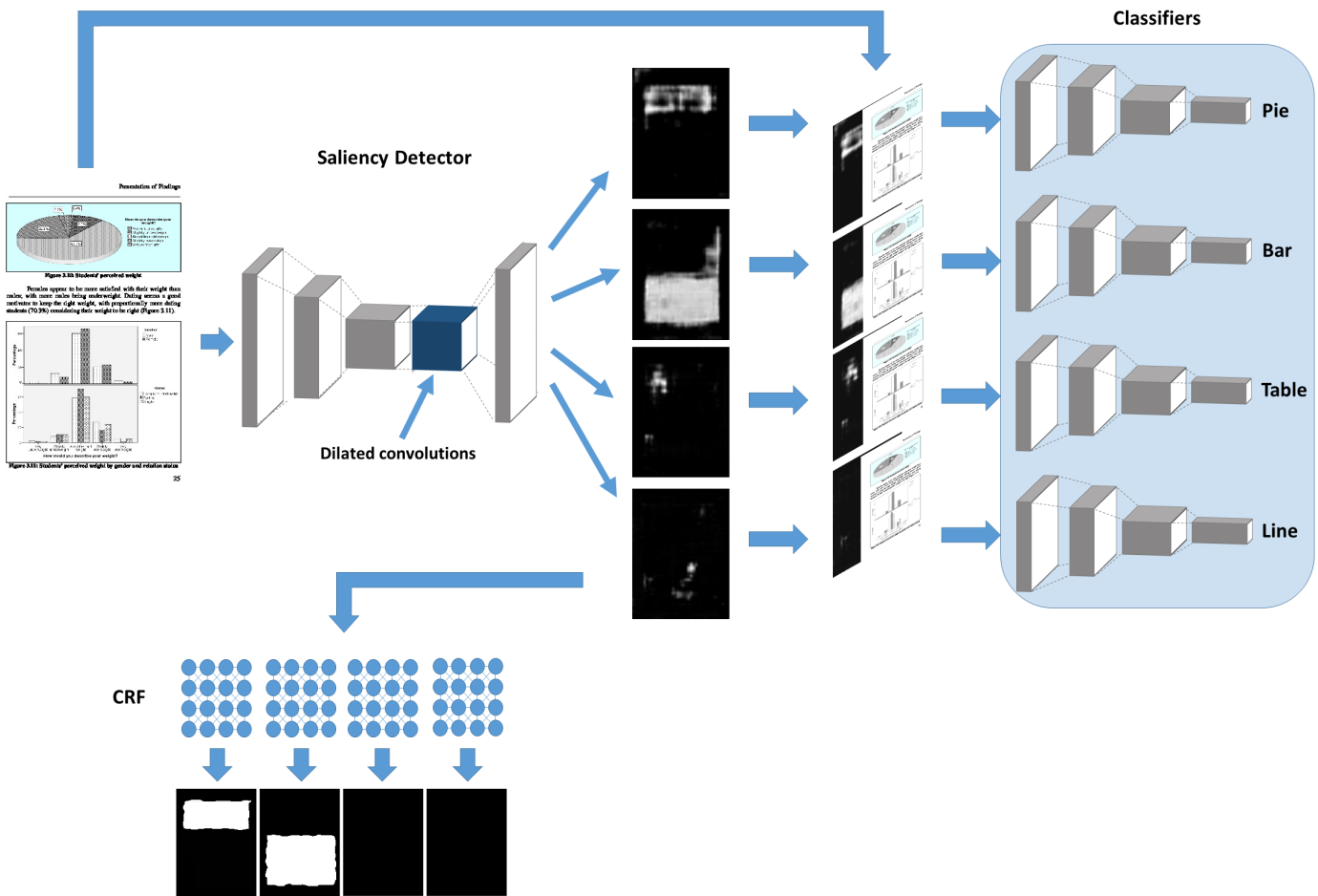


Fig. 2. The proposed system. An input document is fed to a convolutional neural network trained to extract class-specific saliency maps, which are then enhanced and smoothed by CRF models. Moreover, binary classifiers are trained to provide an additional loss signal to the saliency detector, based on how useful the computed saliency maps are for classification purposes.

being the number of object classes, 4 in our case) and the corresponding ground-truth mask \mathbf{T} (same size) is given by the mean squared error between the two:

$$\mathcal{L}_S(\mathbf{Y}, \mathbf{T}) = \frac{1}{N \cdot h \cdot w} \sum_{k=1}^N \sum_{i=1}^h \sum_{j=1}^w (Y_{kij} - T_{kij})^2 \quad (1)$$

where h and w are the image height and width (in our case, both are 300), and Y_{kij} and T_{kij} are the values of the respective tensors at location (i, j) of the k -th saliency map.

The binary classifiers are first trained separately from the saliency network, so that they can be used to provide a reliable error signal to the saliency detector. Training is performed using original images cropped with ground-truth annotations. For example, for training the table classifier, we use table annotations (available in the ground truth) and crop input images so as to contain only tables: these are the “positive samples”. “Negative samples” are, instead, obtained by cropping the original images with annotations from other classes (pie chart, bar chart and line chart) or with random background regions. This procedure is performed for each classifier to be trained. Since cropping may result in images of different sizes, all images are resized to 299×299 to fit the size required by the Inception network.

Each classifier is trained to minimize the negative log-likelihood loss function:

$$\mathcal{L}_{C_i}(\mathbf{I}, t_i) = -t_i \log C_i(\mathbf{I}) - (1 - t_i) \log (1 - C_i(\mathbf{I})) \quad (2)$$

where C_i ($1 \leq i \leq 4$) is the classifier for the i th object class, and returns the likelihood that an object of the targeted class is present in image \mathbf{I} : t_i is the target label, and is 1 if i is the correct class, 0 otherwise. After training the classifiers, they are used to compute the classification loss for the saliency detector, as follows:

$$\mathcal{L}_C = \sum_{i=1}^N \mathcal{L}_{C_i}(\mathbf{I}, t_i) \quad (3)$$

The saliency detector, in this way, is pushed to provide accurate segmentation maps so that whole object regions are passed to the downstream classifiers. Indeed, if the saliency detector is not accurate enough in identifying tables, it will provide incomplete tables to the corresponding classifier, which may be then misclassified as non-table objects with a consequent increase in loss. Note that while training the saliency detector, the classifiers themselves are not re-trained, and are only used to compute the classification loss. This prevents the binary classifiers to learn to recognize objects from their parts, thus

forcing the saliency network to keep improving its detection performance.

The multi-loss used for training the network in an end-to-end manner is, thus, given by the sum of the terms \mathcal{L}_C and \mathcal{L}_S :

$$\mathcal{L} = \mathcal{L}_C + \mathcal{L}_S \quad (4)$$

C. Mask enhancement by Fully-Connected Conditional Random Fields

The outputs of our fully convolution network, usually, show irregularities such as spatially-close objects fused in one object or one object oversegmented in multiple parts. Improving noisy segmentation maps has been usually tackled with conditional random fields (CRFs) [48], which enforce same-label assignments to spatially close pixels. Recently, combining CRFs with deep convolutional networks has gained increased interest to enhance segmentation outputs [49], [50]. In particular, in these methods, fully-connected CRFs [49] are used to recover object structures rather than smoothing segmentation outputs, as instead performed by previous methods based on short-range CRFs. Building on the advantages provided by fully-connected CRFs, we integrate in our system a downstream module based on the architecture proposed in [51], which has demonstrated good capabilities in recovering or significantly mitigating segmentation errors. In detail, the fully-connected CRF module adopts the following energy function:

$$E(x, z) = \sum_i \theta_i(x_i, z_i) + \sum_{ij} \theta_{ij}(x_i, x_j) \quad (5)$$

with $x_i, x_j \in \mathcal{X}$, which is the latent space of pixel label assignment. As unary potential $\theta_i(x_i)$ we employ the label probability likelihood of pixel i provided by the upstream CNN, i.e., the output of the saliency detection network. The pairwise potential is computed, similarly to [52], as:

$$\theta_{ij}(x_i, x_j) = \mu(x_i, x_j) \cdot \left[w_1 \cdot e^{\left(-\frac{\|s_i - s_j\|^2}{2\sigma_\alpha^2} - \frac{\|c_i - c_j\|^2}{2\sigma_\beta^2}\right)} + w_2 \cdot e^{\left(-\frac{\|s_i - s_j\|^2}{2\sigma_\gamma^2}\right)} \right] \quad (6)$$

$\mu(x_i, x_j) = 1$ if $x_i \neq x_j$, i.e. in case the two pixels have different labels, otherwise 0, as in the Potts model [53]. s_i, c_i are, respectively, the spatial coordinates and RGB color values of pixel i , and s_j, c_j the same values for pixel j . The kernel controlled by the w_1 weight takes into account the visuo-spatial distances between the two pixels in order to force pixels with similar colors and spatially close to get the same label. The kernel controlled by w_2 depends only on the spatial distance, thus enforcing smoothness between close pixels. $\sigma_\alpha, \sigma_\beta$ and σ_γ are the kernel widths. Gaussian kernel is used for two main reasons: a) it enforces smoothness in learning the function controlling the data; b) it is suitable to efficient approximate probabilistic inference in fully-connected graphs [8]. It has to be noted that CRF-based output enhancing is performed independently for each mask computed by the saliency detector.

An example of input images and the corresponding intermediate and final outputs is shown in Fig. 3.

IV. PERFORMANCE ANALYSIS

A. Dataset

Training data collection. To train our method, we developed a web crawler that searched and gathered images from Google Images, using the following queries: “tables in documents”, “pie charts”, “bar charts”, “line charts”. Retrieved documents were then converted to images, resulting in 50,466 images available for training.

Test data collection. The dataset used for testing the models was the standard ICDAR 2013 dataset [54]. However, in its original form, ICDAR 2013 does not contain annotations on other graphical elements than tables. Since our method deals also with such other types of graphical elements, we extended the ICDAR 2013 dataset by annotating also pie, line and bar charts.

Post-processing. Given the nature of the method employed for gathering the training dataset, we had to ensure that none of the retrieved images was already contained in the test set. To avoid duplication between training and test sets, we computed HOG features for all available images (training and test) and applied *k*-Nearest Neighbours, with $k = 10$, for similarity search in the two sets. This led to the removal of 24 images from the training set, for a remaining total of 50,442 training images.

Annotations and splits. The annotation of chart objects in training and test images was carried out by paid annotators using an adapted version of the annotation tool in [55]. In particular, among the 50,442 retrieved images only 19,564 had at least one object of interest, while the remaining 30,878 images did not. The 19,564 images with positive instances had in total 22,544 annotations, whose distribution is given in Table II. Of the set of retrieved images (and related annotations), 10% were used as a validation set for model selection, while the remaining 90% as training set. The distribution of instances of the four target classes between the training and validation sets were approximately equal.

As for the test dataset, only 161 out of 238 images from ICDAR 2013 contained objects of interest. In these 161 images, there were 156 tables (with annotations already available) and 58 charts (of either “pie”, “bar” and “line” types), as shown again in Table II.

The training dataset is subject to license restrictions and cannot be published. The extended ICDAR 2013 dataset is publicly available and can be found at <http://perceive.dieei.unict.it>.

TABLE II
TRAINING, VALIDATION AND TEST DATASETS

	Web gathered			ICDAR 2013
	Train	Validation	Total	Test
Tables	8,780	976	9,756	156
Pie charts	1,889	210	2,099	9
Bar charts	5,129	570	5,699	29
Line charts	4,491	499	4,990	20
Total annotations	20,289	2,255	22,544	214
Total images	45,398	5,044	50,442	238

B. Training details, pre- and post-processing

Since the number of annotations in the training set is not enough to avoid overfitting, we pre-trained (100 epochs) our saliency detector on the SALICON dataset [37], containing saliency data of human subjects while visualizing natural images. The binary classifiers were initialized using the weights of the Inception network pre-trained on the ImageNet dataset [56], except for the final classification layer, which is trained from scratch. After the initial pre-training phase, the saliency detector and the classifiers were trained in an end-to-end fashion using an image as input and a) the annotation masks as training targets for the saliency detector, and b) presence/absence labels of target objects on image crops for the classifiers. The input image resolution was set to 300×300 pixels. The training phase ran for 45 epochs, which in our experiments was the point where the performance of the saliency network on the validation set stopped improving.

All networks were trained using the Adam optimizer [57] (learning rate was initialized to 0.001, momentum to 0.9 and batch size to 32).

CRF training was decoupled from the saliency-based network training. In particular, after training our saliency CNN, we computed the CRF unary terms and used them for CRF training, for which we used the code in [51]. Parameters w_1 , w_2 , σ_α , σ_β and σ_γ were set, respectively, to 5, 3, 50, 3, 3.

The deep-learning models were trained using three Titan X Pascal video cards. The CRF models were trained on a server with two 8-core Intel Xeon processors and 128 GB of memory.

C. Performance metrics

Our evaluation phase aimed at assessing the performance of our DCNN in localizing precisely tables and charts in digital documents, as well as in detecting and segmenting table/chart areas.

- **Table/chart localization performance.** To test localization performance we computed precision Pr , recall Re and F_1 score by calculating true positives, false positives and false negatives. A true positive (TP) was identified when a bounding box detected by our approach overlapped (over a threshold value) a ground truth annotation. A false positive (FP) was instead defined as an object detected by our method that did not sufficiently overlap a corresponding annotation in the ground truth. A false negative (FN) was an object present in the ground truth that was not detected by our method (see Fig. 1). Then, precision, recall and F_1 score are calculated as follows:

$$Pr = \frac{TP}{TP + FP} \quad (7)$$

$$Re = \frac{TP}{TP + FN} \quad (8)$$

$$F_1 = \frac{2 \times Pr \times Re}{Pr + Re} \quad (9)$$

- **Segmentation accuracy** was measured by intersection over union (IOU). While the detection scores above represent the ability of the models to detect the tables and charts that overlap with the ground truth over a

certain threshold, IOU measures per-pixel performance by comparing the exact number of the pixels that were detected as belonging to a table or chart. In other words, the IOU score reflects the accuracy in finding the correct boundaries of table and chart regions. IOU is computed by comparing the segmentation mask M_O provided by our model, and the corresponding ground truth mask M_{GT} as follows:

$$IOU_O = \frac{M_O \cap M_{GT}}{M_O \cup M_{GT}}. \quad (10)$$

Higher IOU score values mean that there is a substantial overlap between the detected table/chart and the annotation. The final IOU score reported in the following results is the average IOU values on all ground truth tables and charts.

The proposed model consists of several functional blocks (saliency detection, binary classification, CRF) which are stacked together for final prediction. In order to assess how each block influenced performance, we carried out an ablation study by calculating the above metrics under the following configurations:

- 1) **SAL**: this is the baseline configuration and refers to using only the saliency network (SAL);
- 2) **SAL-CRF**: this configuration, instead, consists of the saliency network followed by the fully-connected CRF;
- 3) **SAL-CL**: saliency detector followed by the binary classifiers;
- 4) **ALL**: the whole system including all parts (saliency detection, CRF and binary classifiers).

D. Results

Table detection performance was tested on the standard ICDAR 2013 dataset, while chart detection performance on the extended ICDAR 2013.

For table/chart localization results, we set IOU = 0.5 as overlap threshold to identify true positives, following common protocols in object detection [58].

The results obtained by the four configurations previously described are reported in Table III. Our system performed very well in all object types, and this performance increased progressively from the baseline configuration (SAL) to the more complex architectures (i.e., SAL-CRF, SAL-CL and ALL). In particular, the baseline configuration (SAL) achieved an average F_1 score of 69.0%, with the top performance achieved on the “Tables” category (76.3%) and the worst on the “Line charts” category (63.4%). The addition of the CRF model (SAL-CRF) to the baseline architecture increased the average F_1 score by about 9%. The increase came mainly through a sharper increase in the recall (i.e., reduction of false negatives) of about 12%, especially for chart objects (e.g., in pie charts the observed increase in recall was more than 22%, which, given the small sample number of pie charts in the test dataset, corresponded to a reduction of the number of false negatives equal to 2). This may be explained by the fact that charts, especially pie charts, have more uniform shapes to start with, so CRFs can easily deduce the correct label given the

saliency map and the input image. Line and bar charts yielded lower performance than pie charts, although the performance was still higher than the baseline. By comparing with the results obtained by SAL-CL model, we can infer that the lower performance was due to the difficulty by the saliency detector alone in extracting discriminative features between these two types of charts.

Indeed, this shortcoming was countered by introducing the classification loss in the model (SAL-CL configuration). The classifiers managed to aid the saliency detector network in recognizing the distinguishing features between line charts (increase to F_1 score of about 24%) and bar charts (increase to F_1 score of about 23%) w.r.t. the baseline, bringing the average F_1 score to 87%.

Finally, testing the whole system (ALL) added a further 6.3% increase to the system’s performance, reaching a maximum average F_1 score of 93.4%. Figures 4 and 5 show examples of, respectively, good and bad detections obtained by our method.

Overall, among the different chart types, pie chart detection was the one that mostly benefited from the CRF module, both because it is more easily distinguishable from bar charts and line charts, and because the relatively closed boundaries of pie charts are easily separable by the CRF’s pairwise potential. For the same reason, the “open” structures of bar and line charts (as well as tables) make it harder to the CRF model to separate white areas belonging to the chart’s region from white areas belonging to the background (e.g., Fig. 6). In these cases, the classification loss introduced with the Inception-based classifiers significantly helped in improving the corresponding accuracy scores.

TABLE III

PERFORMANCE — IN TERMS OF PRECISION, RECALL, F_1 AND IOU — ACHIEVED BY THE DIFFERENT CONFIGURATIONS OF OUR METHOD ON THE EXTENDED ICDAR 2013 DATASET. VALUES ARE IN PERCENTAGE.

Configuration	Class	Precision	Recall	F_1	IOU
SAL	Tables	78.38	74.36	76.32	65.28
	Pie charts	75.00	66.67	70.59	62.67
	Bar charts	62.50	68.97	65.57	63.45
	Line charts	61.90	65.00	63.41	62.10
	Average	69.45	68.75	68.97	63.37
SAL-CRF	Tables	81.88	83.97	82.91	71.39
	Pie charts	80.00	88.89	84.21	73.11
	Bar charts	73.33	75.86	74.58	68.55
	Line charts	68.00	73.91	70.83	67.87
	Average	75.80	80.66	78.13	70.23
SAL-CL	Tables	93.79	87.18	90.37	75.51
	Pie charts	87.50	77.78	82.35	72.22
	Bar charts	86.67	89.66	88.14	76.38
	Line charts	89.47	85.00	87.18	74.75
	Average	89.36	84.90	87.01	74.72
ALL	Tables	97.45	98.08	97.76	81.33
	Pie charts	100	88.89	94.12	78.11
	Bar charts	90.00	93.10	91.53	79.59
	Line charts	90.00	90.00	90.00	78.50
	Average	94.36	92.52	93.35	79.38

To ground our work with state of the art in table detection, we compared the performance of the four different configurations of our method to those achieved by DeepDeSRT [59], Tran [34] and Hao [27] in detecting only tables on the ICDAR

2013 dataset. The comparison is reported in Table IV and highlights the importance of the different components of our method. In the SAL configuration, the performance achieved were the lowest ($F_1 = 76.3\%$), meaning that generic saliency detection alone was not enough to completely extract all the information necessary to identify tables. There was a mild increase in performance when the CRF module was added (SAL-CRF configuration), where an increase of more than 6% in F_1 score was observed ($F_1 = 82.9\%$). The increase was even more substantial when the classifiers were included in the configuration (SAL-CL), where an increase of 14% in F_1 score was observed (90.4%). When all components were included in the experiment (ALL configuration), our system achieved an F_1 score of 97.8%, outperforming the state-of-the-art methods.

TABLE IV
COMPARISON OF STATE OF THE ART METHODS IN TABLE DETECTION ACCURACY ON THE STANDARD ICDAR 2013 DATASET

	Table Detection		
	Precision	Recall	F_1
DeepDeSRT [59]	97.4	96.1	96.7
Tran [34]	95.2	96.4	95.8
Hao [27]	97.2	92.2	94.6
SAL	78.4	74.4	76.3
SAL-CRF	81.9	83.4	82.9
SAL-CL	93.8	87.2	90.4
Our method (ALL)	97.5	98.1	97.8

What was clear from the results was that CRF-based approaches influence the number of false negatives and subsequently, the recall, more than they influence the number of false positives. In fact, w.r.t. the baseline configuration, the CRF module added a modest 6% in precision, but 12% in recall. This was explained by the fact that the major contribution of CRF models consisted in filling gaps and holes resulting from the deep learning methods, especially for very large tables with large white areas.

V. CONCLUSION

The identification of graphical elements such as tables and charts in documents is an essential processing block for any system that aims at extracting information automatically. In this paper, we presented a method for automatic table and chart detection in document files converted to images, hence without exploiting format information (e.g., PDF tokens or HTML tags) that limit the general applicability of these approaches. The core of our model is a DCNN trained to detect salient regions from document images, with saliency based on the categories of objects that we aim to identify (tables, pie charts, bar charts, line charts). An additional loss signal based on the generated saliency maps’ discriminative power in a classification task was provided during training, and a fully-connected CRF model was finally employed to smooth and enhance the final outputs. Performance evaluation, carried out on the standard ICDAR 2013 benchmark and on an extended version with additional annotations of charts, showed that the proposed model achieves better performance than state-of-the-art methods in the localization of tables and charts.

Appendix A - Glossary

Table A-1. Summary of forecast assumptions to 2021

Variable	Assumption
Demographic assumptions	
Population	Projections are consistent with the Census Bureau's estimates.
15- to 24-year-old population	Census Bureau projection: average annual growth rate of 0.1%
25- to 39-year-old population	Census Bureau projection: average annual growth rate of 0.1%
40- to 54-year-old population	Census Bureau projection: average annual growth rate of 0.1%
55- to 64-year-old population	Census Bureau projection: average annual growth rate of 0.1%
Economic assumptions	
Disposable income per capita in constant dollars	Annual percent changes range between -1.0% and 2.3% with an annual growth rate of 1.4%
Education research results from state education per capita in constant dollars	Annual percent changes range between -2.4% and 2.3% with an annual growth rate of 1.2%
Inflation rate	Inflation rate ranges between 1.0% and 2.0%
Unemployment rate (mean)	
Age 16 and 19	Remains between 17.7% and 18.8%
Age 20 to 24	Remains between 10.9% and 10.9%
Age 25 and over	Remains between 5.3% and 7.9%
Unemployment rate (median)	
Age 16 and 19	Remains between 14.5% and 16.9%
Age 20 to 24	Remains between 6.5% and 10.1%
Age 25 and over	Remains between 5.0% and 7.3%

As the Census Bureau projections used in this report do not include the 2011 Census Bureau population estimates, the Census Bureau's population projections for each year were updated by multiplying the ratio of the total Census Bureau estimates for 2011 to the total Census Bureau estimates for 2010. SOURCE: U.S. Department of Commerce, Census Bureau, Population Estimates, released October 18, 2011, <http://www.census.gov/ipeds/data/cen2010/states.html>; U.S. Department of Commerce, Census Bureau, Population Projections, released November 2, 2010, <http://www.census.gov/ipeds/data/cen2010/projections.html>; U.S. Department of Commerce, Census Bureau, Inflation, released October 18, 2011, <http://www.bls.gov/charts/inflation.html>; U.S. Monthly Retail Sales, released January 27, 2012, <http://www.bls.gov/charts/retail-sales.html>.

Table A-2. Salary in 1994, 1997, and 2003

Category	1994	1997	2003
Lowest	\$0,596 or less	\$22,400 or less	\$34,000 or less
Lower middle	\$0,995 - \$1,992	\$22,401 - \$29,992	\$34,001 - \$48,000
Upper middle	\$17,993 - \$23,771	\$29,993 - \$40,000	\$48,001 - \$66,000
Highest	Greater than \$23,771	Greater than \$40,000	Greater than \$66,000

In 1994, respondents reported the annual salary or rate of pay for the job they held in April 1994 (AFRANSAL). When the salary in 1994 appears as a new variable, it is based on SALPCT, which is the percentage of respondents who reported the salary in 1994 (B2SALARY) is the respondent's annual salary for the job held in April 1997 (except for teachers, for whom the academic-year salary was used). Salary in 2003 (B2SALARY) is the respondent's annual salary for his or her current (teacher's class) or most recent job (for teaching teachers). In 2003, respondents who reported salaries greater than \$500,000 were included in \$500,000.

B2SALARY has a weighted item response rate to be 83 percent when the entire survey sample is considered (as in table 1), thus requiring a data analysis according to NESS publication standards; see appendix B for details on how this report's findings might have been biased due to missing data on B2SALARY.

Table A-3. Monthly loan payment in 1997

Monthly loan payment as a percentage of monthly income, created by dividing the monthly student loan payment amount by monthly income and multiplying by 100. The percentages were multiplied by 100 to achieve higher precision—specifically, to be able to show median debt burden to one decimal place rather than an integer. Respondents with unrealistically high values (i.e., a debt burden of more than 50 percent) were excluded from the analysis of debt burden in this report; less than 1 percent were excluded for this reason. This variable includes payments for both undergraduates and graduate loans in 1997. However, when used in this report, the amount refers to payments on undergraduate loans only because only bachelor's degree recipients with no additional degree credentials were included in the analysis of debt burden.

The monthly income refers to income from all sources in 1996, the year prior to the Survey of Income, Program Participation, and Income Sources (SIPP) survey for both 1994 (B2PCT12) and 2003 (B2PCT13). For the other years, income refers to salary income in the survey year (see details under "B2PCT12" and "B2PCT13" in this glossary). The impact of this difference on findings in this report is minimal because B2PCT12 was used only in table 1 and was used only as a new variable.

APPENDIX A

HIGHLIGHTS FROM PIRLS 2011

Table A-3. Number and percentage distribution of reading items in the PIRLS assessment, by content

Content domain and process	All items		New items		Total items	
	Number	Percent	Number	Percent	Number	Percent
Total items	125	100	60	100	75	100
Purposes of reading						
Library experience	72	53	33	55	36	52
Accept and use information	63	47	27	45	36	48
Processes of comprehension						
Focus on and retrieve explicitly stated information	33	24	14	23	10	25
Make straightforward inferences	46	34	20	33	26	35
Integrate and evaluate ideas and information	38	28	18	30	20	27
Examine and evaluate content, language, and textual elements	18	13	8	13	10	13

NOTE: The number of items in this table does not equal the total number of items in the assessment because some items are used in more than one reading category.

Design of instruments

The booklets were rotated a month students, with each participating student completing one booklet only. The reading items were each assembled separately into 10 books, or clusters, of items. Each of the 13 PIRLS 2011 booklets contained two books in total. Each booklet contained one block of literary experience items and one block of informational items only and each book contained items across the 13 booklets. Six of the ten books we included in previous PIRLS assessments. The remaining four books were new for PIRLS 2011.

The PIRLS 2011 included booklets containing assessment items as well as so-called "background" questionnaires for principals, teachers, and students. This is consistent with other large scale assessments, such as NAEP.

The 2011 assessment consisted of 12 booklets, and one reader (presented in a magazine-type format with the questions in a separate booklet). The assessment is given in 40-minute parts with a 5- to 10-minute break in between. The student questionnaire given after the second part of the assessment, while untimed, is allotted approximately 30 minutes of response time.

As part of the design process, it was necessary to ensure that the booklets showed an item distribution across the reading content domains as specified in the framework as well as a relatively equal distribution of items by item type. The number of reading items in the PIRLS 2011 assessment is shown in table A-4.

Table A-4. Number and percentage of reading items in the PIRLS assessment, by item format, 2011

Item Format	Number of Items	Percent of Items
Total	125	100
Multiple choice	74	59
Constructed response	51	41

SOURCE: International Association for the Evaluation of Educational Achievement (IEA), Progress in International Reading Literacy Study (PIRLS), 2011.

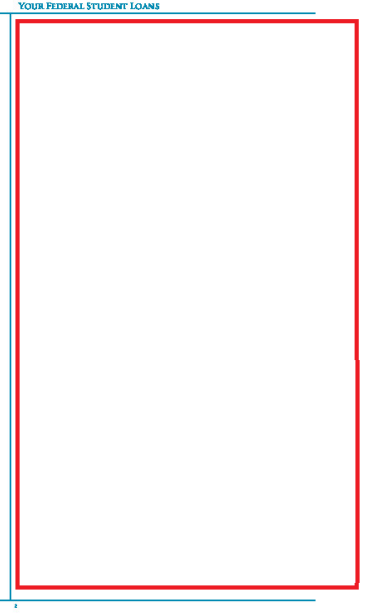
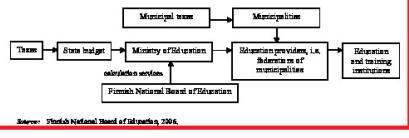


Fig. 5. Examples of bad detections by our method. *Top row, false negatives:* A partially detected unruled table (left), a completely undetected unruled table (middle) and a page with two tables where one was not detected at all (the small one near the bottom). *Bottom row, false positives:* A complete white area that was recognized as a table (middle), the model was confused from the vertical and horizontal blue lines present in the same page, a flow diagram that was classified as a bar chart (middle) and an image that was classified as a line chart (left, partially).

10. Financing: investment in human resources

10.1. Background information

Figure 6. Simplified chart of flows of funding of TVET in Finland (training provided by federations of municipalities)

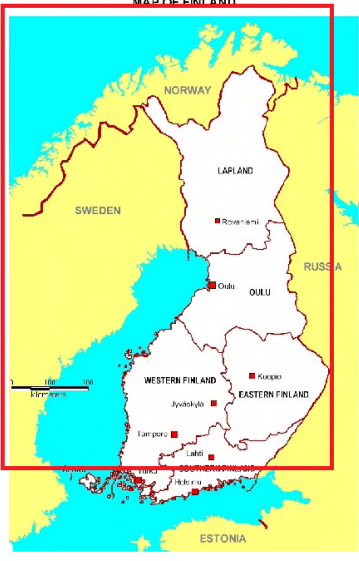


The Ministry of Education is responsible for funding education and training (see Annex 3, Aot 634/1998 on the Financing of Educational and Cultural Provisions) except for labour market training which is the responsibility of the Ministry of Labour. Responsibility for educational funding and capital expenditure is divided between the State and local authorities. The funding criteria are the same irrespective of ownership. Labour market training is mainly purchased by the labour authorities from the different training providers (see Glossary) but there can also be joint labour and education authority measures for training the employed.

Vocational education and training are primarily financed through public funds. This will continue to be the case, although there are continuing discussions about increasing the share of financial contributions from employers and individuals.

Decentralisation of educational administration has been a key aspect of education policy since the 1990s. Decision-making has been increasingly handed over by central government to education providers. This also applies to funding: education providers have relatively extensive powers to decide on the use of their funds. In recent years, attention has also focused on the effectiveness and quality of vocational education and training.

Funding received from the European Union has diversified the funding model for vocational education and training. EU funding is mainly used to finance development projects related to upper secondary and vocational further education and training (see Glossary). In addition, EU aid is allocated to training intended for the unemployed.



July 2017.

[2] J. Li, Y. Wei, X. Liang, J. Dong, T. Xu, J. Feng, and S. Yan, "Attentive contexts for object detection," *IEEE Transactions on Multimedia*, vol. 19, no. 5, pp. 944–954, May 2017.

[3] S. Ren, K. He, R. Girshick, and J. Sun, "Faster r-cnn: Towards real-time object detection with region proposal networks," in *Advances in neural information processing systems*, 2015, pp. 91–99.

[4] R. Girshick, "Fast r-cnn," in *The IEEE International Conference on Computer Vision (ICCV)*, December 2015.

[5] L. Itti, C. Koch, and E. Niebur, "A model of saliency-based visual attention for rapid scene analysis," *IEEE Transactions on Pattern Analysis and Machine Intelligence*, vol. 20, no. 11, pp. 1254–1259, Nov 1998.

[6] F. Yu and V. Koltun, "Multi-scale context aggregation by dilated convolutions," in *International Conference on Learning Representations*, 2016.

[7] F. Murabito, C. Spampinato, S. Palazzo, D. Giordano, K. Pogorelov, and M. Riegler, "Top-down saliency detection driven by visual classification," *Computer Vision and Image Understanding*, 2018. [Online]. Available: <http://www.sciencedirect.com/science/article/pii/S1077314218300407>

[8] P. Krähenbühl and V. Koltun, "Efficient inference in fully connected crfs with gaussian edge potentials," in *Advances in Neural Information Processing Systems 24*, J. Shawe-Taylor, R. S. Zemel, P. L. Bartlett, F. Pereira, and K. Q. Weinberger, Eds. Curran Associates, Inc., 2011, pp. 109–117. [Online]. Available: <http://papers.nips.cc/paper/4296-efficient-inference-in-fully-connected-crf-with-gaussian-edge-potentials.pdf>

[9] J. Chen and D. Lopresti, "Table detection in noisy off-line handwritten documents," in *Document Analysis and Recognition (ICDAR), 2011 International Conference on*. IEEE, 2011, pp. 399–403.

3. INFORMATION ON SPECIFIC ZOONOSES

Figure CA1 | Age-specific distribution of reported confirmed cases of human campylobacteriosis, 7855 cases for reporting 2007

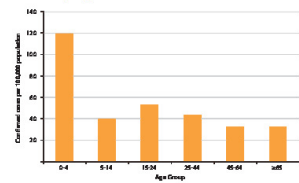
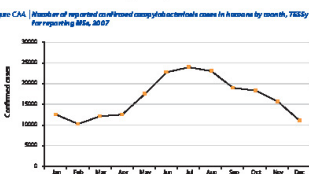


Figure CA2 | Number of reported confirmed campylobacteriosis cases in humans by month, 7855 cases for reporting 2007

The most frequently reported campylobacter species in 2007 was *C. jejuni* (84.7%), while *C. coli* accounted for 2.7% of campylobacter isolates. Other species, including *C. coli* (0.7%), accounted for 8.9% of the isolates. Forty-six percent of 394,563 campylobacter isolates were not specified or were unknown.

14 | The IEEE Journal of Multimedia - 2020

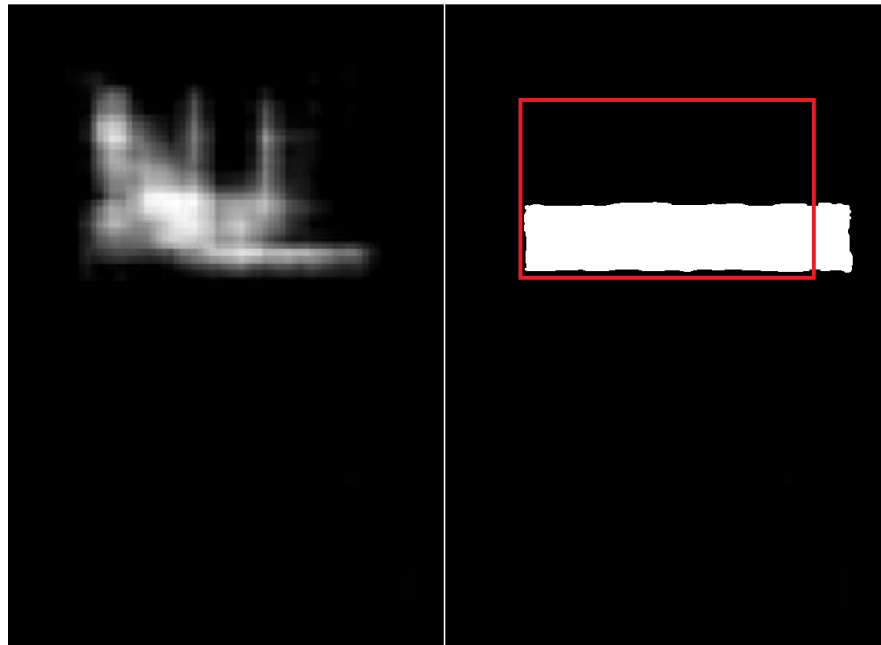


Fig. 6. Partial detection of a bar chart by the network. The network correctly identified the most salient regions of the chart (middle) but failed to expand the detection's boundaries to cover it completely. The output shown in the middle, is the normalized result of the network before the CRF model was applied. The final output of the model is the white rectangle (right). The red bounding box represents the ground truth.

- [10] J. Fang, L. Gao, K. Bai, R. Qiu, X. Tao, and Z. Tang, "A table detection method for multipage pdf documents via visual separators and tabular structures," in *Document Analysis and Recognition (ICDAR), 2011 International Conference on*. IEEE, 2011, pp. 779–783.
- [11] F. Shafait and R. Smith, "Table detection in heterogeneous documents," in *Proceedings of the 9th IAPR International Workshop on Document Analysis Systems*. ACM, 2010, pp. 65–72.
- [12] B. Gatos, D. Danatsas, I. Pratikakis, and S. J. Perantonis, "Automatic table detection in document images," in *International Conference on Pattern Recognition and Image Analysis*. Springer, 2005, pp. 609–618.
- [13] S. Deivalakshmi, K. Chaitanya, and P. Palanisamy, "Detection of table structure and content extraction from scanned documents," in *Communications and Signal Processing (ICCSPP), 2014 International Conference on*. IEEE, 2014, pp. 270–274.
- [14] B. Krüpl, M. Herzog, and W. Gatterbauer, "Using visual cues for extraction of tabular data from arbitrary html documents," in *Special interest tracks and posters of the 14th international conference on World Wide Web*. ACM, 2005, pp. 1000–1001.
- [15] B. Krüpl and M. Herzog, "Visually guided bottom-up table detection and segmentation in web documents," in *Proceedings of the 15th international conference on World Wide Web*. ACM, 2006, pp. 933–934.
- [16] M. A. Jahan and R. G. Ragel, "Locating tables in scanned documents for reconstructing and republishing," in *Information and Automation for Sustainability (ICIAfS), 2014 7th International Conference on*. IEEE, 2014, pp. 1–6.
- [17] Y. Liu, P. Mitra, and C. L. Giles, "Identifying table boundaries in digital documents via sparse line detection," in *Proceedings of the 17th ACM conference on Information and knowledge management*. ACM, 2008, pp. 1311–1320.
- [18] M. Raskovic, N. Bozidarevic, and M. Sesum, "Borderless table detection engine," Jan. 23 2012, uS Patent App. 13/521,424.
- [19] W. Huang, C. L. Tan, and W. K. Leow, "Model-based chart image recognition," in *International Workshop on Graphics Recognition*. Springer, 2003, pp. 87–99.
- [20] M. Shao and R. P. Futrelle, "Recognition and classification of figures in pdf documents," in *International Workshop on Graphics Recognition*. Springer, 2005, pp. 231–242.
- [21] W. Huang, R. Liu, and C.-L. Tan, "Extraction of vectorized graphical information from scientific chart images," in *Document Analysis and Recognition, 2007. ICDAR 2007. Ninth International Conference on*, vol. 1. IEEE, 2007, pp. 521–525.
- [22] V. Karthikeyani and S. Nagarajan, "Machine learning classification algorithms to recognize chart types in portable document format (pdf) files," *International Journal of Computer Applications*, vol. 39, no. 2, 2012.
- [23] M. O. Perez-Arriaga, T. Estrada, and S. Abad-Mota, "Tao: System for table detection and extraction from pdf documents," in *FLAIRS Conference*, 2016, pp. 591–596.
- [24] S. Shetty, H. Srinivasan, M. Beal, and S. Srihari, "Segmentation and labeling of documents using conditional random fields," in *Document Recognition and Retrieval XIV*, vol. 6500. International Society for Optics and Photonics, 2007, p. 65000U.
- [25] A. Delaye and C.-L. Liu, "Text/non-text classification in online handwritten documents with conditional random fields," in *Chinese Conference on Pattern Recognition*. Springer, 2012, p. 514–521.
- [26] D. Pinto, A. McCallum, X. Wei, and W. B. Croft, "Table extraction using conditional random fields," in *Proceedings of the 26th annual international ACM SIGIR conference on Research and development in informaion retrieval*. ACM, 2003, pp. 235–242.
- [27] L. Hao, L. Gao, X. Yi, and Z. Tang, "A table detection method for pdf documents based on convolutional neural networks," in *Document Analysis Systems (DAS), 2016 12th IAPR Workshop on*. IEEE, 2016, pp. 287–292.
- [28] M. Z. Afzal, S. Capobianco, M. I. Malik, S. Marinai, T. M. Breuel, A. Dengel, and M. Liwicki, "Deepdocclassifier: Document classification with deep convolutional neural network," in *Document Analysis and Recognition (ICDAR), 2015 13th International Conference on*. IEEE, 2015, pp. 1111–1115.
- [29] L. Kang, J. Kumar, P. Ye, Y. Li, and D. Doermann, "Convolutional neural networks for document image classification," in *Pattern Recognition (ICPR), 2014 22nd International Conference on*. IEEE, 2014, pp. 3168–3172.
- [30] S. Roy, A. Das, and U. Bhattacharya, "Generalized stacking of layerwise-trained deep convolutional neural networks for document image classification," in *Pattern Recognition (ICPR), 2016 23rd International Conference on*. IEEE, 2016, pp. 1273–1278.
- [31] X. Liu, B. Tang, Z. Wang, X. Xu, S. Pu, D. Tao, and M. Song, "Chart classification by combining deep convolutional networks and deep belief networks," in *Document Analysis and Recognition (ICDAR), 2015 13th International Conference on*. IEEE, 2015, pp. 801–805.
- [32] B. Tang, X. Liu, J. Lei, M. Song, D. Tao, S. Sun, and F. Dong, "Deepchart: Combining deep convolutional networks and deep belief networks in chart classification," *Signal Processing*, vol. 124, pp. 156–161, 2016.

- [33] A. Gilani, S. R. Qasim, and F. Malik, Imran abd Shafait, "Table detection using deep learning," in *Document Analysis and Recognition (ICDAR), 2017 16th International Conference on*. IEEE, 2017.
- [34] D. N. Tran, T. A. Tran, A. Oh, S. H. Kim, and I. S. Na, "Table detection from document image using vertical arrangement of text blocks," *International Journal of Contents*, vol. 11, no. 4, pp. 77–85, 2015.
- [35] G. Li and Y. Yu, "Visual saliency detection based on multiscale deep cnn features," *IEEE Transactions on Image Processing*, vol. 25, no. 11, pp. 5012–5024, 2016.
- [36] M. Kümmerer, L. Theis, and M. Bethge, "Deep gaze i: Boosting saliency prediction with feature maps trained on imagenet," *arXiv preprint arXiv:1411.1045*, 2014.
- [37] M. Jiang, S. Huang, J. Duan, and Q. Zhao, "Salicon: Saliency in context," in *Computer Vision and Pattern Recognition (CVPR), 2015 IEEE Conference on*. IEEE, 2015, pp. 1072–1080.
- [38] S. He, R. W. Lau, W. Liu, Z. Huang, and Q. Yang, "Supercnn: A superpixelwise convolutional neural network for salient object detection," *International journal of computer vision*, vol. 115, no. 3, pp. 330–344, 2015.
- [39] N. Liu and J. Han, "Dhsnet: Deep hierarchical saliency network for salient object detection," in *Computer Vision and Pattern Recognition (CVPR), 2016 IEEE Conference on*. IEEE, 2016, pp. 678–686.
- [40] Y. Li, K. Fu, Z. Liu, and J. Yang, "Efficient saliency-model-guided visual co-saliency detection," *IEEE Signal Processing Letters*, vol. 22, no. 5, pp. 588–592, 2015.
- [41] R. Zhao, W. Ouyang, H. Li, and X. Wang, "Saliency detection by multi-context deep learning," in *Proceedings of the IEEE Conference on Computer Vision and Pattern Recognition*, 2015, pp. 1265–1274.
- [42] J. Pan, E. Sayrol, X. Giro-i Nieto, K. McGuinness, and N. E. O'Connor, "Shallow and deep convolutional networks for saliency prediction," in *Proceedings of the IEEE Conference on Computer Vision and Pattern Recognition*, 2016, pp. 598–606.
- [43] A. Almahairi, N. Ballas, T. Cooijmans, Y. Zheng, H. Larochelle, and A. Courville, "Dynamic capacity networks," in *Proceedings of the 33rd International Conference on International Conference on Machine Learning - Volume 48*, ser. ICML'16. JMLR.org, 2016, pp. 2549–2558. [Online]. Available: <http://dl.acm.org/citation.cfm?id=3045390.3045659>
- [44] J. Yao, S. Fidler, and R. Urtasun, "Describing the scene as a whole: Joint object detection, scene classification and semantic segmentation," in *2012 IEEE Conference on Computer Vision and Pattern Recognition*, June 2012, pp. 702–709.
- [45] J. Long, E. Shelhamer, and T. Darrell, "Fully convolutional networks for semantic segmentation," in *Proceedings of the IEEE conference on computer vision and pattern recognition*, 2015, pp. 3431–3440.
- [46] K. Simonyan and A. Zisserman, "Very deep convolutional networks for large-scale image recognition," *ICLR 2015*, vol. abs/1409.1556, 2014.
- [47] C. Szegedy, W. Liu, Y. Jia, P. Sermanet, S. Reed, D. Anguelov, D. Erhan, V. Vanhoucke, A. Rabinovich *et al.*, "Going deeper with convolutions." *Cvpr*, 2015.
- [48] P. Kohli, P. H. Torr *et al.*, "Robust higher order potentials for enforcing label consistency," *International Journal of Computer Vision*, vol. 82, no. 3, pp. 302–324, 2009.
- [49] L.-C. Chen, G. Papandreou, I. Kokkinos, K. Murphy, and A. L. Yuille, "Deeplab: Semantic image segmentation with deep convolutional nets, atrous convolution, and fully connected crfs," *arXiv preprint arXiv:1606.00915*, 2016.
- [50] F. Liu, G. Lin, and C. Shen, "Crf learning with cnn features for image segmentation," *Pattern Recognition*, vol. 48, no. 10, pp. 2983–2992, 2015.
- [51] P. Krähenbühl and V. Koltun, "Efficient inference in fully connected crfs with gaussian edge potentials," in *Advances in neural information processing systems*, 2011, pp. 109–117.
- [52] L. Chen, G. Papandreou, I. Kokkinas, K. Murphy, and A. Yuille, "Semantic image segmentation with deep convolutional nets and fully connected crfs," *ICLR 2015*, vol. abs/1412.7062, 2015.
- [53] F.-Y. Wu, "The potts model," *Reviews of modern physics*, vol. 54, no. 1, p. 235, 1982.
- [54] D. Karatzas, F. Shafait, S. Uchida, M. Iwamura, L. G. i Bigorda, S. R. Mestre, J. Mas, D. F. Mota, J. A. Almazan, and L. P. de las Heras, "Icdar 2013 robust reading competition," in *Document Analysis and Recognition (ICDAR), 2013 12th International Conference on*. IEEE, 2013, pp. 1484–1493.
- [55] I. Kavasidis, S. Palazzo, R. Di Salvo, D. Giordano, and C. Spampinato, "An innovative web-based collaborative platform for video annotation," *Multimedia Tools and Applications*, vol. 70, no. 1, pp. 413–432, 2014.
- [56] J. Deng, W. Dong, R. Socher, L.-J. Li, K. Li, and L. Fei-Fei, "Imagenet: A large-scale hierarchical image database," in *Computer Vision and Pattern Recognition, 2009. CVPR 2009. IEEE Conference on*. IEEE, 2009, pp. 248–255.
- [57] D. Kingma and J. Ba, "Adam: A method for stochastic optimization," *arXiv preprint arXiv:1412.6980*, 2014.
- [58] M. Everingham, L. Van Gool, C. K. Williams, J. Winn, and A. Zisserman, "The pascal visual object classes (voc) challenge," *International journal of computer vision*, vol. 88, p. 303–338, 2010.
- [59] S. Schreiber, S. Agne, I. Wolf, A. Dengel, and S. Ahmed, "Deepdesrt: Deep learning for detection and structure recognition of tables in document images," in *Document Analysis and Recognition (ICDAR), 2017 14th IAPR International Conference on*, vol. 1. IEEE, 2017, pp. 1162–1167.